Sensors and Materials, Vol. 34, No. 7 (2022) 2541–2553
MYU Tokyo

S & M 2989

SF_6 Arc Extinction Sensor Design for Substation Mechanical Equipment in Smart Grid

Qian Huang, Pengdan Ge, and Nina Dai*

School of Electronics and Information Engineering, Chongqing Three Gorges University, Chongqing 404130, China

(Received December 30, 2021; accepted April 26, 2022)

Keywords: non-dispersive IR, error compensation, gray wolf optimization–radial basis function, SF_6 arc extinction sensor, high-voltage substation

An SF_6 arc extinction sensor (AES) has the advantages of wide measurement, high sensitivity, and strong anti-interference ability, and has a wide range of applications in high-voltage substations. To effectively monitor and control SF_6 gas in substation mechanical equipment, we have designed an SF_6 AES based on non-dispersive IR (NDIR). However, in the actual measurement, temperature and air pressure differences in the environment affect the detection accuracy of the device, and an appropriate method of eliminating the measurement error caused by changes in the environment is required. In this paper, we propose the use of a gray wolf optimization-radial basis function (GWO-RBF) neural network to compensate for the measurement error caused by temperature and pressure changes. The experimental results show that the SF_6 concentration error after the GWO-RBF algorithm is ±15 ppm in the concentration range of 0–2000 ppm and the full-scale error is 0.75%. Compared with uncompensated data and radial basis function (RBF) compensation methods, the proposed GWO-RBF algorithm effectively enhances the measurement accuracy and stability of the AES, allowing its volume and cost to be reduced.

1. Introduction

Because of its excellent chemical stability, good insulation, and arc extinction properties, SF_6 gas is as ideal insulation and arcing medium after air and insulating oil, and it is widely used in high-pressure electric power equipment, including circuit breakers and transformers. The use of SF_6 in power devices is effective for reducing the volume and failure rate of the equipment.(1) However, in the operation of high-pressure electric power equipment, SF_6 gas is easily decomposed by a high-temperature arc or spark discharge, generating a variety of toxic and harmful substances. These substances may corrode metals used in the power equipment, which can accelerate the degradation of the insulation, reduce the insulation strength, reduce the electrical performance of the equipment, and even endanger the lives of power maintenance personnel in severe cases.(2) Therefore, accurate, convenient, and rapid measurement of the SF_6

*Corresponding author: e-mail: dainina83@163.com
https://doi.org/10.18494/SAM3835

ISSN 0914-4935

gas concentration is conducive to maintaining the safe operation of power equipment and ensuring the safety of operators.

Currently, the main approaches for detecting the SF_6 gas concentration include electronic capture, laser imaging, the use of a high-pressure negative current, an electrochemical method, UV ionization, and a non-dispersive IR absorption method.[3–5] Moreover, non-dispersive IR (NDIR)-based gas detection applies the feature absorption peak at 10.55 μm in the IR band waveband corresponding to SF_6 gas molecules to achieve the quantitative detection of SF_6 gas concentrations in combination with the Lambert–Beer (LB) law. This approach has the advantages of a long service life and high stability, detection accuracy, and detection speed. However, the detection accuracy of an NDIR SF_6 arc extinction sensor (AES) is reduced by changes in the surrounding environmental air pressure in actual application. Two compensation schemes are mainly used to eliminate the effects of environmental pressure fluctuations on an NDIR-based SF_6 AES. First, a formula-based method, i.e., a least-squares iterative method, is used to determine the correlation coefficient of the fitting formula, establish a mathematical model, and realize air pressure compensation for the SF_6 AES.[6] However, this method uses the coefficient calibration method after data acquisition, making the calculation process complicated. Second, a constant-voltage compensation method is used to eliminate the measurement error of the AES caused by the variation of air pressure, i.e., the hardware circuit module allows the pressure of the detection environment air to maintain a dynamic balance. However, this method requires an additional hardware circuit in the system, which not only increases the power consumption and manufacturing cost but also reduces the reliability of the devices.[7]

In this paper, we propose the use of a software-based algorithm, i.e., the gray wolf optimization-radial basis function (GWO-RBF) neural network algorithm, to compensate for changes in the air pressure and temperature of a SF_6 gas concentration detecting device. By using the absolute error between the measured data and the predicted value, we demonstrate that the GWO-RBF neural network algorithm can eliminate the deviation of the detected value due to changes in the environmental temperature and air pressure, and improve the detection accuracy of the SF_6 AES.

2. Testing Principle of NDIR

The spectrum line of many asymmetric diatoms and polyatomic gas molecules is in the IR band, and when IR radiation of different wavelengths passes through the gas medium to be tested, the gas molecules selectively absorb the energy of the specific band. If the energy is exactly equal to the difference between the two energy levels of the gas molecule, the corresponding energy level transition is triggered and the corresponding absorption peak appears in the characteristic spectrum.[8] SF_6 gas has strong absorbance at a wavenumber of 947 cm^{-1} (10.55 μm wavelength) according to the HITRAN database, and its absorption line is shown in Fig. 1.

The measurement accuracy of an NDIR-based SF_6 AES is mainly based on the following two aspects. The ideal gas state equation is defined as

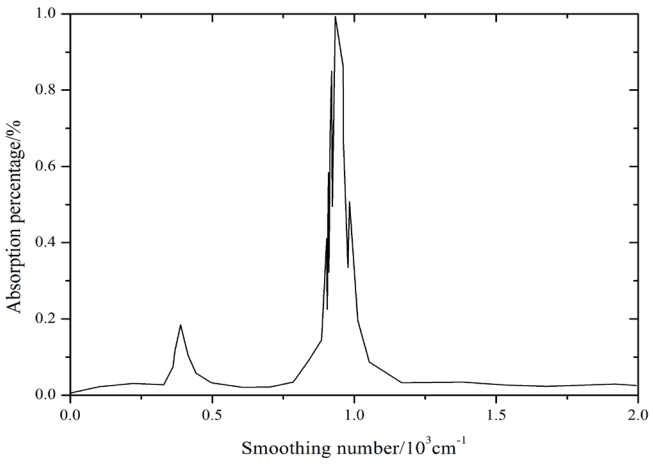

Fig. 1. SF_6 gas absorption spectrum.

$$PV = M \cdot R \cdot T\,, \tag{1}$$

where P is the pressure of the ideal gas, V is the amount of the ideal gas, M is the molar mass of the ideal gas, R is the ideal gas constant, and T is the absolute temperature of the ideal gas. The volume of the tested SF_6 gas changes with P, resulting in a loss of measurement accuracy. On the other hand, fluctuations of the air pressure change the range of IR light wavelength coverage of the light source, which affects its luminescence strength and causes a measurement error of the sensor.

For wavelength λ, $I_{in}(\lambda)$ represents the initial light intensity, and the interaction between gas molecules and IR light causes the attenuation of IR light intensity to $I_{out}(\lambda)$. The decrease in the light intensity follows the LB law,[9] which is expressed as

$$I_{out}(\lambda) = I_{in}(\lambda) e^{-\mu CL}\,. \tag{2}$$

Here, μ is the absorption coefficient of the IR light at the corresponding wavelength, C is the concentration of the gas to be tested, and L is the optical path length of the IR light through the gas. In the measurement, the gas to be tested strongly absorbs the IR light in the measurement channel, whereas there is no absorption of the IR light in the reference channel. From Eq. (2), the output light intensity of the measured channel can be obtained as

$$I_{out}^{m}(\lambda) = I_{in}^{m}(\lambda) e^{-\mu_m \cdot C \cdot L}\,. \tag{3}$$

The output light intensity of the reference channel is

$$I_{out}^{r}(\lambda) = I_{in}^{r}(\lambda) e^{-\mu_r \cdot C \cdot L}\,. \tag{4}$$

In the experiment, the optical paths of the measured channel and reference channel originate from the same light source, and the initial light intensities in the two channels are almost equal, i.e., $I_{in}^{m}(\lambda) \approx I_{in}^{r}(\lambda)$. By dividing Eq. (3) by Eq. (4), the concentration C of the tested gas can be obtained as

$$C = \frac{1}{L[\mu_r - \mu_m]} \ln \frac{I_{out}^{m}(\lambda)}{I_{out}^{r}(\lambda)}. \tag{5}$$

The differential detection technique can obtain the concentration of the gas to be tested because both the measured optical path and the reference optical path are in the same analysis chamber and detection environment, and the use of the reference optical path effectively eliminates external factors such as light source jitter and optical device contamination, and improves the detection accuracy and stability of the SF_6 AES.[10]

3. SF_6 AES

The performance of the SF_6 AES is closely related to the optical path structure, which directly affects the measurement accuracy of AES.[11,12] Therefore, the employed optical path structure is a single chamber with a dual wavelength as shown in Fig. 2. After the IR radiation emitted by the wide-spectrum IR light source passes through the analyzing gas chamber, the SF_6 gas under test passes through a reference filter with λ_r = 3.95 μm and a measured filter with λ_m = 10.55 μm, and is received and analyzed at a double-element thermal release detector (e.g., PYS3228TC/G7.4/G20). The SF_6 gas has no effect on the absorption of IR radiation of wavelength $I(\lambda_r)$, and its output electrical signal does not contain information on the SF_6 gas concentration. However, the SF_6 gas strongly absorbs IR radiation of wavelength $I(\lambda_m)$, and the intensity of its output electrical signal is closely related to the SF_6 gas concentration.

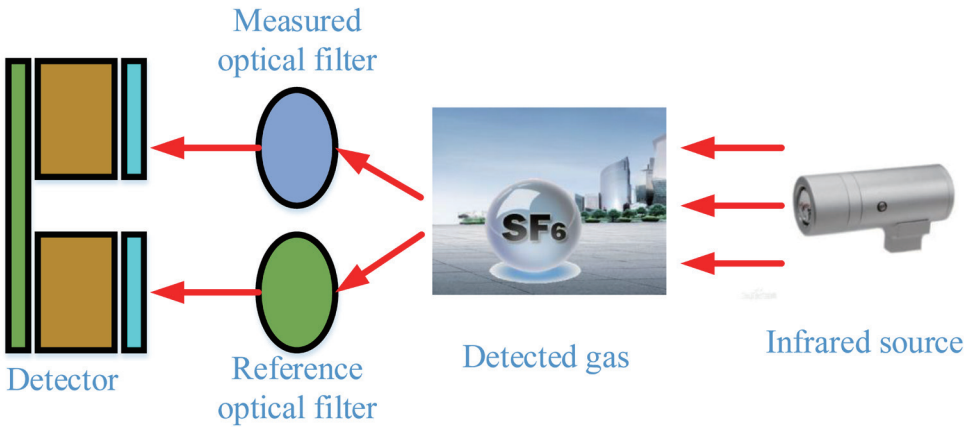

Fig. 2. (Color online) Gas detection model.

4. GWO-RBF Neural Network Compensation Algorithm

4.1 GWO algorithm

The GWO algorithm is a novel intelligent optimization algorithm that simulates the population system, hunting process, and predation behavior of the gray wolf.[13] It is assumed that a wolf group consists of 5 to 12 gray wolves, in which the adaptivity can be divided into four levels, α, β, δ, and η. In the predatory process, α, β, and δ wolves continuously pursue prey while changing their positions, and the remaining gray wolves η follow the α, β, and δ wolves. The optimized solution is the specific location of the prey. Owing to the uncertainty of the position of each gray wolf, the distance between each gray wolf and the prey is expressed as

$$D(t) = \left|\sigma \cdot p(t) - X(t)\right|, \tag{6}$$

where t is the number of iterations, and $p(t)$ and $X(t)$ define the positions of the prey and the gray wolf at iteration t, respectively. In addition, $\sigma = 2A$, where A is a random number in [0,1]. The positions of the gray wolves $X_\alpha(0)$, $X_\beta(0)$, $X_\delta(0)$, and $X_\eta(0)$ are randomly initialized then updated as follows:

$$\begin{cases} X(t+1) = p(t) - A(t)D(t), \\ A(t) = 2a(t) \cdot B - a(t), \\ a(t) = 2 - 2\left(\dfrac{t}{max}\right), \end{cases} \tag{7}$$

where B is a random number in [0,1] $a(t)$ is the convergence factor, and max is the maximum number of iterations. For the α, β, and δ wolves, the following equations are satisfied:

$$\begin{cases} D_\alpha = \left|C_1 \cdot X_\alpha(t) - X(t)\right|. \\ D_\beta = \left|C_1 \cdot X_\beta(t) - X(t)\right|. \\ D_\delta = \left|C_1 \cdot X_\delta(t) - X(t)\right|. \\ X_1 = X_\alpha - A_1 \cdot D_\alpha. \\ X_2 = X_\beta - A_1 \cdot D_\beta. \\ X_3 = X_\delta - A_1 \cdot D_\delta. \end{cases} \tag{8}$$

From Eq. (8), the location of a η gray wolf in the next generation is defined as

$$X_\eta(t+1) = \frac{X_1 + X_2 + X_3}{3}. \tag{9}$$

4.2 RBF algorithm

Owing to its strong nonlinear mapping ability and excellent generalization capacity, the RBF neural network is applied to compensate for data collected by gas sensors. Its principle is based on the organization structure and operation mechanism of the human brain, and a large number of interconnected processing units are used to simulate and explore the intelligent technology of the human brain structure and function.[14,15] The RBF neural network consists of three parts: the first layer is an input layer, the second layer is a hidden layer, in which the number of nodes is determined according to the optimization needs, and the third layer is an output layer, whose output vector is Y, i.e., the value predicted by a sensor after processing by a neural network. The structure of the RBF neural network is shown in Fig. 3.

The Gaussian function is selected as the excitation function of the RBF neural network, which can be defined as

$$R(\|dist\|) = \exp\left(-\frac{1}{2\theta^2}\|x_p - c_i\|^2\right), \tag{10}$$

where θ is the variance of the Gaussian function, x_p is the neural network input sample, c_i is the node center of the hidden layer, and $\|x_p - c_i\|$ defines the Euclidean norm. The orthogonal least-squares algorithm is used as a training algorithm for the RBF neural network, and the number of nodes in the hidden layer is determined by the gradual growth method. The output function of the j (j = 1, 2, ..., m)th node is expressed as

$$\varphi(j) = \exp\left(-\frac{1}{2\theta^2}\|x_p - c_i\|^2\right). \tag{11}$$

Finally, the following RBF neural network model is applied to the pressure compensation of an SF_6 AES:

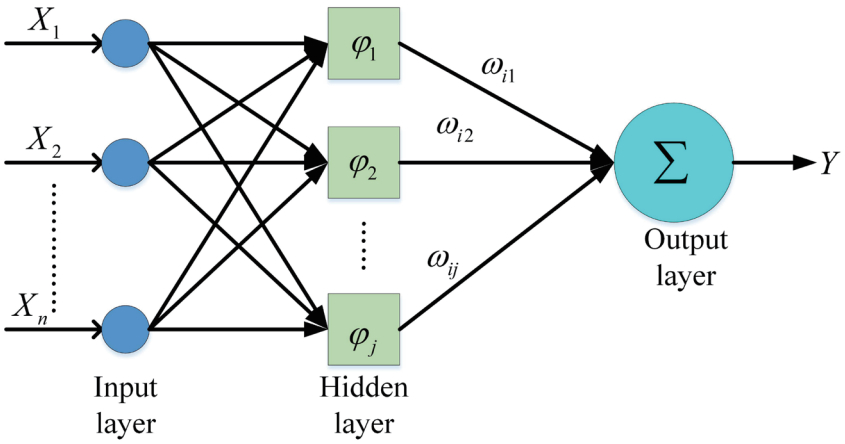

Fig. 3. (Color online) RBF neural network structure.

$$y_i = \sum_{j=1}^{m} \varphi(j) \cdot W_{ij}, \tag{12}$$

where m is the number of nodes in the hidden layer (experimentally determined to be 15 in this study) and W_{ij} is the connection weight between the hidden layer and the output layer.

4.3 GWO-RBF neural network algorithm

The convergence speed of the RBF neural network is low, making it easy for it to fall into a local minimum value. Therefore, we use the GWO algorithm to strengthen the global search capability. As shown in Fig. 4, the positions of the gray wolves serve as the weight of the RBF neural network, the GWO algorithm performs several iterations, and the position of the prey is updated by the algorithm, i.e., the threshold of the RBF neural network is constantly updated, allowing global optimal results to be calculated. The steps of the algorithm are as follows:

Step 1: Select appropriate training data. In this paper, the output voltage ratio of the measured channel to the reference channel, the gas concentration data, the corresponding air pressure, and the temperature are employed as the training data.

Step 2: Construct the RBF neural network model. The number of input layers is n and the number of hidden layers is m, in which the number of neuron nodes is q ($q = \sqrt{n+m} + a$, $a \in [1,10]$). a is a constant in [1,10] and is set to 5 after multiple trials, for which the convergence speed and fitting accuracy are highest.

Step 3: Initialize the GWO optimization algorithm. The optimal positions X_a, X_β, and X_δ in the current iteration are initialized.

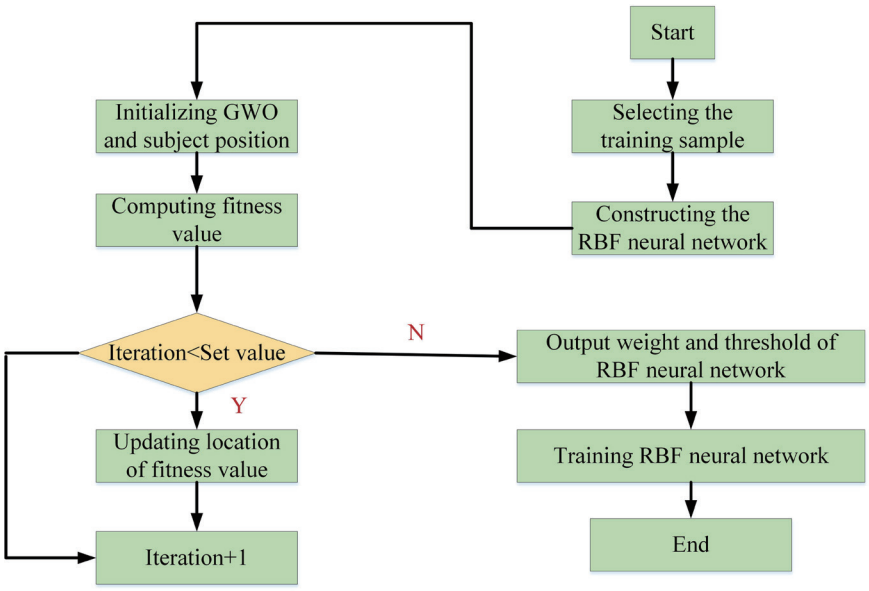

Fig. 4. (Color online) Flowchart of hybrid GWO-RBF neural network.

Step 4: Calculate the fitness value of each individual. The weight and threshold of the RBF neural network are the objects used to solve the GWO algorithm. The sum of the errors of each neural node of the RBF neural network is used as the fitness function of the positions of individuals in the GWO optimization algorithm to obtain the position with the current best fitness value.
Step 5: When the number of iterations reaches the upper limit, the GWO optimization algorithm ends, and the best initial weight and threshold of the RBF neural network are obtained.
Step 6: The RBF neural network performs network training and performance evaluation according to the weight and threshold optimized by the GWO algorithm, and finally obtains the prediction results.

5. Results and Discussion

In the establishment of the GWO-RBF neural network, we used MATLAB simulation software to update the individual positions in the GWO algorithm until the number of iterations reached the set value. As shown in Fig. 5, the optimal fitness value was achieved within 500 iterations during temperature compensation, and after 500 iterations, the fitness value was close to zero, thus demonstrating the potential of the GWO to find the best initial weight and threshold of the RBF neural network.[16] The relationship between the iteration number and fitness value during air pressure compensation over 500 iterations is also shown in Fig. 5.

5.1 Data collection

We performed an experiment in which SF_6 with a concentration of 2000 ppm is mixed with 99.9% purity N_2. Under the standard atmosphere, the gas entered the gas chamber through the flow meter, and then the homogeneous gas mixture entered the SF_6 AES. The initial

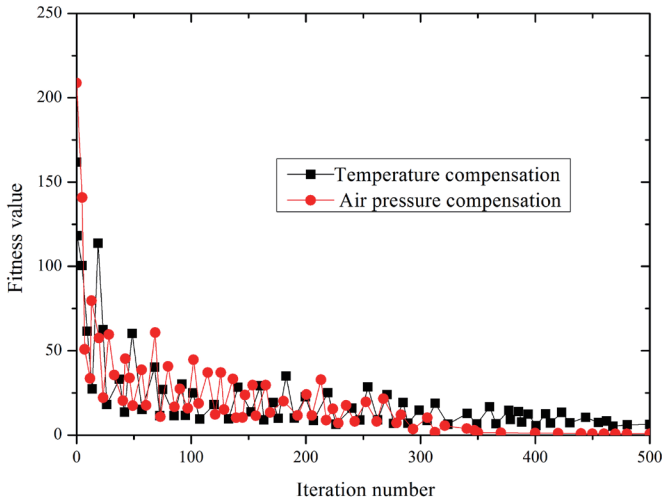

Fig. 5. (Color online) Relationship between iteration number and fitness value.

concentration of gas was 0 ppm, and the SF_6 gas of 2000 ppm required for the experiment was obtained by adjusting the flow rate of the flow meter. The AES sensor was placed in the temperature test chamber and pressure test chamber for data collection.

During the acquisition of data for temperature compensation, the temperature of the test chamber was sequentially adjusted to 10, 15, 20, 25, 30, 35, and 40 ºC. At each temperature, different concentrations of gas were transferred into the SF_6 AES chamber, then the voltages of the measured channel and reference channel were recorded after 3 min. Data were acquired 10 times for each air temperature and concentration, and the average value was taken.

During the acquisition of data for air pressure compensation, the air pressure in the laboratory was adjusted to 100 kPa. At each air pressure, different concentrations of gas were input into the AES sensor, then data were recorded after 3 min. Data were acquired 10 times for each air temperature and concentration, and the average value was taken.

5.2 Compensation analysis

The compensation of the temperature and air pressure was performed using the acquired data, where 20 and 15 data sets were collected as samples, respectively, and the compensation neural network was constructed. The effect of the ambient temperature and pressure on the gas concentration was clearly reduced after compensation and the measurement accuracy of the sensor was improved, indicating effective compensation.

During the temperature compensation, the collected 20 sets of data were first processed. The output voltage ratio of the measured channel to the reference channel of the AES and the corresponding temperature value were used as the input variables of the GWO-RBF neural network, and the SF_6 gas standard concentration was given as the output vector; thus, a neural network structure with two inputs and a single output was constructed. After the prediction by the GWO-RBF neural network, the output vector was a concentration value. The gas concentration curves before and after the temperature compensation are shown in Fig. 6. The

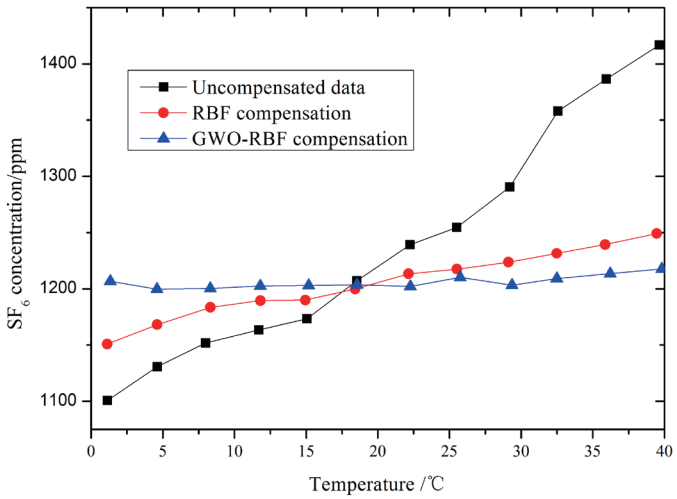

Fig. 6. (Color online) Results of temperature compensation.

data collected from the 1200 ppm concentration were compensated by the RBF neural network and the GWO-RBF neural network and compared with the data without temperature compensation. The black curve in Fig. 6 shows the concentration without uncompensated data; when the environmental temperature was continuously increased, the measured concentration gradually increased. The red curve shows the concentration with compensation of the RBF neural network; it can be seen that the concentration offset was appropriately reduced. The blue curve shows the concentration with compensation of the GWO-RBF neural network. It can be seen from Fig. 6 that the concentration offset of the GWO-RBF neural network was significantly reduced, and the slope of each concentration curve is almost zero. During the entire temperature change, the offset of the gas concentration was no more than ±15 ppm. The GWO-RBF neural network can provide more effective compensation and higher measurement accuracy than the cases of RBF compensation and no compensation of the data.

When compensating for the air pressure, the 15 acquired data sets were first preprocessed to obtain the data used to train the GWO-RBF neural network, and a neural network for air pressure compensation was constructed. The structure was the same as that of the temperature compensation network, with two inputs and a single output. After the input data were processed by the GWO-RBF neural network, the gas concentration after air pressure compensation was output. Figure 7 shows the concentration curves of 1200 ppm SF_6 gas before and after compensation. As can be seen from Fig. 7, without air pressure compensation, there is a small difference between the measured SF_6 gas concentration at 100 kPa and the actual value. As the air pressure increases, the offset of the measured value gradually increases. Upon the air pressure compensation of the GWO-RBF neural network, the measured value of the gas concentration is significantly reduced, and the offset of the gas concentration does not exceed ±15 ppm. Compared with the compensation by the RBF neural network, the compensation by the GWO-RBF neural network is more accurate in the entire concentration range and the compensation is more effective.

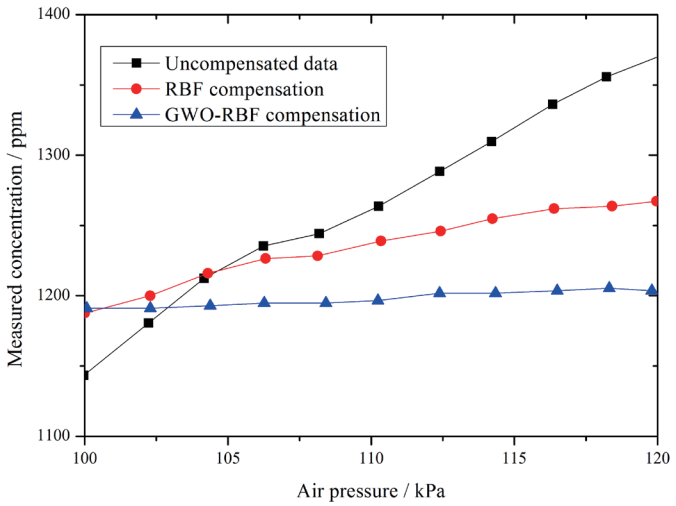

Fig. 7. (Color online) Measured concentration for the different algorithms.

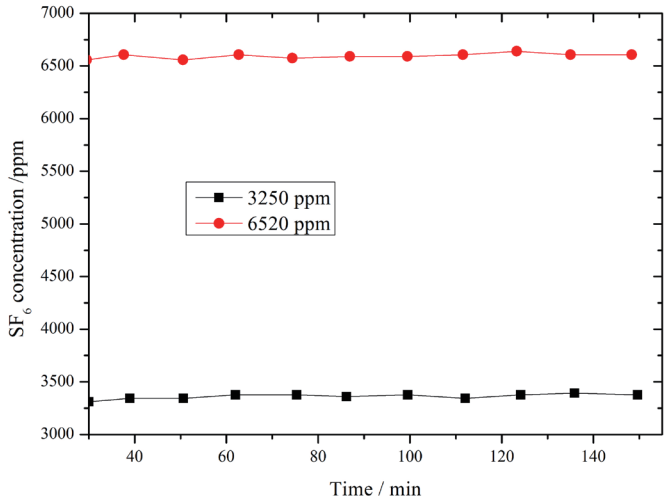

Fig. 8. (Color online) Results of stability test of hybrid GWO-RBF neural network.

5.3 Stability test

We also tested the stability of an SF_6 AES. The SF_6 AES was placed in a constant-pressure test chamber with the initial air pressure set to 100 kPa. The stability of the AES output results was monitored using SF_6 gases with concentrations of 3250 and 6520 ppm. Figure 8 shows the stability test results for the two concentrations of SF_6 gases over 150 min. For both concentrations, the fluctuation of the result output by the SF_6 AES was small and the error was less than ±400 ppm, indicating the stability of the AES.

6. Conclusions

The measurement accuracy of an SF_6 AES is susceptible to changes in the temperature and air pressure. In this study, we used a GWO-RBF neural network to compensate for the differences caused by fluctuations in the temperature and air pressure. Owing to the high convergence speed of the GWO, its strong global search performance, and its ability to avoid falling into a local optimum, the GWO was combined with the RBF neural network to overcome its shortcomings. Compared with the traditional hardware-based circuit compensation method, the proposed compensation method is the more stable and effective, and it is conducive to the miniaturization of the AES. The experimental results show that the offset of the gas concentration based on the compensation method is ±15 ppm in the SF_6 concentration range of 0–2000 ppm. The full-scale error was 0.75%, which means that the GWO-RBF neural network can use the temperature and air pressure for effective compensation in the gas detection process, greatly reducing the effects of temperature and air pressure on the measurement accuracy of the SF_6 AES.

Acknowledgments

This work was supported by the Science and Technology Project of Chongqing Education Commission (Nos. KJQN201901213 and KJZD-K201901203) and Natural Science Foundation of Chongqing Municipality (No. cstc2021jcyj-msxm2025).

References

1 Y. He, W. Ding, A. Sun, and G. Zhang: IEEE Trans. Dielectr. Electr. Insul. **28** (2021) 829. https://doi.org/10.1109/TDEI.2021.9450688
2 D. Yang, F. Zeng, X. Yang, J. Tang, Q. Yao, Y. Miao, and L. Chen: IEEE Trans. Dielectr. Electr. Insul. **25** (2018) 863. https://doi.org/10.1109/TDEI.2018.006701
3 H. Tachikawa and T. Yamano: Chem. Phys. **264** (2001) 81. https://doi.org/10.1016/S0301-0104(00)00393-1
4 K. Kuhn, E. Pignanelli, and A. Schutze: IEEE Sens. J. **13** (2013) 934. https://doi.org/10.1109/JSEN.2012.2224104
5 F. Zeng, Z. Lei, X. Yang, J. Tang, Q. Yao, and Y. Miao: IEEE Trans. Power Delivery **34** (2019) 1383. https://doi.org/10.1109/TPWRD.2019.2900508
6 L. Zhang, T. Zhang, and H.-S. Shin: IEEE Sens. J. **21** (2021) 10122. http://doi.org/10.1109/JSEN.2021.3057448
7 J. Lu, G. Zhu, D. Lin, Y. Zhang, H. Wang, and C. C. Mi: IEEE Trans. Intell. Transp. Syst. **22** (2021) 600. https://doi.org/10.1109/TITS.2020.2985658
8 Q. Tan, L. Tang, M. Yang, C. Xue, W. Zhang, J. Liu, and J. Xiong: Opt. Lasers Eng. **74** (2015) 103. https://doi.org/10.1016/j.optlaseng.2015.05.007
9 A. Gobrecht, R. Bendoula, J. M. Roger, and V. Bellon-Maurel: Anal. Chim. Acta. **853** (2015) 486. https://doi.org/10.1016/j.aca.2014.10.014
10 X. Wang, D. Wang, Z. Liu, T. Lan, and M. Rong: IEEE Electron Device Lett. **41** (2020) 1408. https://doi.org/10.1109/LED.2020.3012693
11 H. Heiermeier and R. B. Raysaha: IEEE Trans. Power Delivery **35** (2020) 691. https://doi.org/10.1109/TPWRD.2019.2922111
12 R. Yang, P. V. Er, Z. Wang, and K. K. Tan: Neurocomputing **199** (2016) 31. https://doi.org/10.1016/j.neucom.2016.01.093
13 S. N. Ghorpade, M. Zennaro, and B. S. Chaudhari: IEEE Trans. Intell. Transp. Syst. **22** (2021) 1217. https://doi.org/10.1109/TITS.2020.2964604
14 A.-K. Seghouane and N. Shokouhi: IEEE Trans. Cybern. **51** (2021) 2847. https://doi.org/10.1109/TCYB.2019.2951811
15 Q. Que and M. Belkin: IEEE Trans. Pattern Anal. Mach. Intell. **42** (2020) 1856. https://doi.org/10.1109/TPAMI.2019.2906594
16 A. K. Mishra, S. R. Das, P. K. Ray, R. K. Mallick, A. Mohanty, and D. K. Mishra: IEEE Access **8** (2020) 74497. http://doi.org/10.1109/ACCESS.2020.2988611

About the Authors

Qian Huang received her B.S. degree from Chongqing Three Gorges University, China, and her M.S. degree in engineering from State Grid Electric Power Research Institute, China, in 2009 and 2012, respectively. In 2012, she joined the Nanrui Group, where she works in R&D and on-site commissioning, and is involved in the National Power Project. In 2015, she joined the School of Electronics and Information Engineering, Chongqing Three Gorges University, where she is an experimentalist. She has served as a member of the Chongqing Women's Science and Technology Workers Association. Her research interests include generator excitation control, power grid fault analysis, and power grid control strategy. (qianhuang512@126.com)

Pengdan Ge received her B.S. degree in automation from Shanxi University, China, in 2020. She is currently pursuing her master's degree in the School of Electronics and Information Engineering, Chongqing Three Gorges University. Her research interests include the technology of connecting electric vehicles to the grid and coding technology. (1362269439@qq.com)

Nina Dai received her B.S. degree in electronic information engineering and her M.S. degree in circuits and systems from Central China Normal University, China. She joined Chongqing Three Gorges University in 2008, where she is an associate professor. Her research interests include communication and coding technology. (dainina83@163.com)